**A. Bhattacharyya**[1]
Senior Technical Staff Member,
Able Corporation,
Yorba Linda, CA

**A. J. Acosta**
Professor Emeritus.

**C. E. Brennen**
Professor and Head.

**T. K. Caughey**
Hayman Professor of
Mechanical Engineering.

Department of Mechanical Engineering,
California Institute of Technology,
Pasadena, CA 91125

# Rotordynamic Forces in Cavitating Inducers

*This paper reports an experimental investigation of rotordynamic forces in a whirling axial flow inducer under the influence of cavitation at various flow coefficients. The results show the occurrence of large destabilizing peaks in the force tangential to the whirl orbit for positive whirl frequency ratios. The magnitude of the destabilizing forces increased with a decrease in cavitation number and flow coefficient. The rotordynamic data obtained do not exhibit quadratic functional behavior normally assumed in many rotordynamic models. Consequently, conventional generalized stiffness, damping, and inertia matrices cannot be determined for the inducer. The results demonstrate the complexity of rotordynamic forces and their consequences on stability of axial flow inducers.*

## Introduction

The purpose of the research presented in this paper is to obtain an insight into the characteristics of fluid-induced rotordynamic forces acting on an axial flow inducer operating under cavitating conditions. Rotordynamic forces arise when the inducer is displaced off-center and whirls in an orbit. These forces are conventionally decomposed into components normal and tangential to the whirl orbit. These forces can be destabilizing depending on whirl speeds and operating conditions. This paper presents experimental dynamic force data for varying whirl speeds, flow coefficients and cavitation numbers. Experiments have been conducted at the Rotor Force Test Facility (RFTF) at the California Institute of Technology to obtain force data on a whirling inducer, for varying conditions of cavitation, flow rates and whirl. An experimental perturbation technique has been used to obtain force data using an eccentric bearing mechanism and a rotating dynamometer for measuring all force components in a rotating frame. The perturbation is introduced in the form of a circular whirl motion created by an offset of the inducer center with respect to the housing centerline. The radius of this whirl orbit can be set to different eccentricities ($\epsilon$). The hydrodynamic force matrix obtained can be used to study the stability of the inducer.

A survey of the literature shows a lack of dynamic force data on whirling cavitating inducers. Some of the early measurements of hydrodynamic radial forces includes a study by Rosenmann (1965) on a three bladed cavitating inducer. Karyeaclis et al. (1989) conducted previous experiments at the RFTF on a four bladed SEP (Sociéte Européene de Propulsion) inducer. Internal flows in inducers change substantially with flow coefficients and affect fluid-induced forces. One such change is the occurrence of reverse flow. These reverse flows occur both upstream as tip clearance leakage flows and downstream as reentrant flow on the hub. The internal blade passage flows become highly complex and three dimensional (Lakshminarayana, 1972, 1982; Acosta, 1993; Bhattacharyya et al., 1993). It has also been shown that upstream swirling backflow can induce instability in the system through low cycle system oscillations (Kamijo et al., 1977); however the force data reported in this paper were taken at operating conditions at which such oscillations were not observed.

The results of the current experiments show the effect of flow coefficient and cavitation number on the rotordynamic and lateral forces and the range of whirl/shaft speed ratios (or whirl frequency ratios) over which they are destabilizing. The results also show a non-quadratic behavior of these forces with the whirl/shaft speed ratio as a consequence of which the conventional rotordynamic stiffness, damping and inertia coefficients cannot be obtained.

## Experimental Procedure

Experiments were conducted in the RFTF to obtain steady (lateral) and unsteady (rotordynamic) force data on a three bladed helical inducer. The inducer has a constant hub/tip ratio and a constant helix pitch of 0.4 and 5.04 cm/revolution respectively. The blade angle is 9° at the tip and the inducer has a swept back leading edge. Further details of the test facility and data acquisition can be found in Jery (1986), Franz (1989) and Franz et al. (1990). A schematic of the inducer installation in the test facility is shown in Fig. 1(*a*).

A brief overview of the data reduction process is presented here; further details can be obtained from Jery (1986). The components of the instantaneous forces on a whirling inducer and the reference frames are shown in Fig. 1(*b*). The instantaneous force $[F]$ can be expressed as the sum of a steady force $[F_o]$ and an unsteady force which is linearized with respect to perturbation, $\epsilon$, represented by $[A]$:

$$\begin{bmatrix} F_x \\ F_y \end{bmatrix} = \begin{bmatrix} F_{ox} \\ F_{oy} \end{bmatrix} + \frac{\epsilon}{R} \begin{bmatrix} A_{xx} & A_{xy} \\ A_{yx} & A_{yy} \end{bmatrix} \begin{bmatrix} \cos \omega t \\ \sin \omega t \end{bmatrix} \quad (1)$$

The components of the rotordynamic matrix $[A]$ for a circular whirl orbit have been experimentally found to be very close to the form $A_{xx} = A_{yy}$ and $A_{xy} = -A_{yx}$. The forces normal to the whirl orbit ($F_n$) and tangential to the whirl orbit ($F_t$) can then be expressed as:

$$F_n = \tfrac{1}{2}(A_{xx} + A_{yy}) = A_{xx} = A_{yy} \quad (2)$$

and

$$F_t = \tfrac{1}{2}(A_{yx} - A_{xy}) = -A_{xy} = A_{yx} \quad (3)$$

[1] Currently: Project Engineer, Concepts ETI, Inc., 4 Billings Farm Rd., White River Jct., VT 05001.

Contributed by the Fluids Engineering Division for publication in the JOURNAL OF FLUIDS ENGINEERING. Manuscript received by the Fluids Engineering Division July 20, 1995; revised manuscript received March 19, 1997. Associate Technical Editor: O. C. Jones.

  

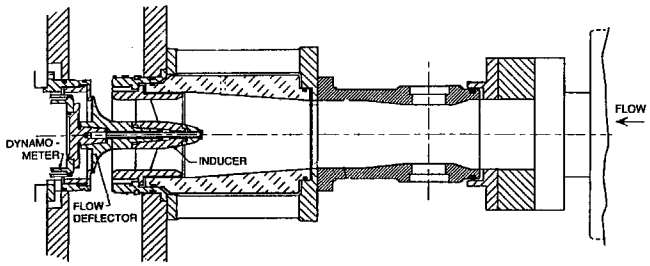


**Fig. 1 (*a*) Schematic of inducer installation in the test facility**

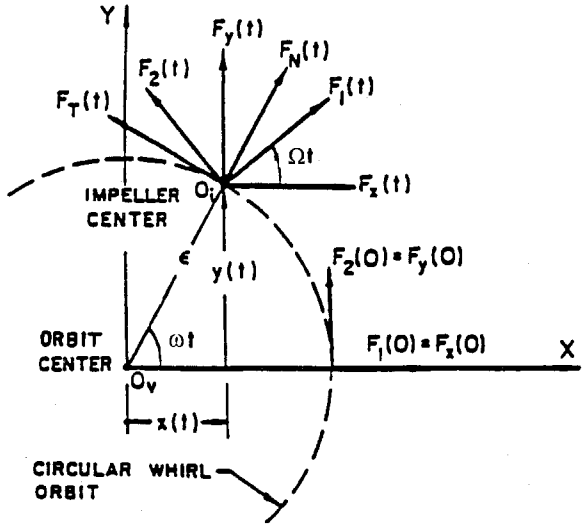


**Fig. 1 (*b*) Schematic showing rotordynamic forces in laboratory and rotating reference frames**

The sign conventions are such that $F_n$ is positive outward and $F_t$ is positive in the direction of rotation. It follows that a *positive* tangential force is destabilizing when the whirl motion is in the same direction as the shaft rotational motion (i.e. a positive whirl/shaft speed ratio). Conversely, a negative $F_t$ tends to stabilize the whirl motion for a positive whirl/shaft speed ratio. Likewise, a positive $F_t$ would be stabilizing for a *negative* whirl motion. In the case of the normal force, a positive (outward) force could be considered as a destabilizing force in the sense that it tends to increase the radius of the whirl orbit.

Rotordynamicists typically characterize these forces in terms of inertia, stiffness and damping matrices for stability analysis in the following manner:

$$\begin{bmatrix} F_x \\ F_y \end{bmatrix} = \begin{bmatrix} F_{ox} \\ F_{oy} \end{bmatrix} - [K]\begin{bmatrix} x \\ y \end{bmatrix} - [C]\begin{bmatrix} \dot{x} \\ \dot{y} \end{bmatrix} - [M]\begin{bmatrix} \ddot{x} \\ \ddot{y} \end{bmatrix} + \textit{higher order terms} \quad (4)$$

The matrices $[K]$, $[C]$, and $[M]$ are the stiffness, damping and inertia matrices respectively. It can be shown that the components of the rotordynamic force matrix $[A]$ can also be expressed in terms of the components of the stiffness, damping and inertia matrices as:

$$A_{xx} = M_{xx}\left(\frac{\omega}{\Omega}\right)^2 - C_{xy}\left(\frac{\omega}{\Omega}\right) - K_{xx}; \quad (5)$$

$$-A_{xy} = M_{xy}\left(\frac{\omega}{\Omega}\right)^2 + C_{xx}\left(\frac{\omega}{\Omega}\right) - K_{xy}; \quad (6)$$

$$A_{yx} = M_{yx}\left(\frac{\omega}{\Omega}\right)^2 - C_{yy}\left(\frac{\omega}{\Omega}\right) - K_{yx}; \quad (7)$$

$$A_{yy} = M_{yy}\left(\frac{\omega}{\Omega}\right)^2 + C_{yx}\left(\frac{\omega}{\Omega}\right) - K_{yy} \quad (8)$$

where $\omega$ is the whirl speed and $\Omega$ is the inducer rotational speed.

The above formulation implies that the coefficients of the stiffness, damping and inertia matrices can be obtained from rotordynamic force data if the forces can be expressed as a quadratic function of $\omega/\Omega$. Rotordynamic forces in centrifugal

## Nomenclature

$A_i$ = inlet cross-sectional area, $\pi r_t^2$

$[A] = \begin{bmatrix} A_{xx} & A_{xy} \\ A_{yx} & A_{yy} \end{bmatrix}$ = rotordynamic coefficient matrix, nondimensionalized by $\rho\pi\Omega^2 r_t^2 l$

$F_o$ = steady lateral force on the inducer nondimensionalized by $\rho\pi\Omega^2 r_t^3 l$

$F_{ox}$, $F_{oy}$ = components of the steady lateral force in the $(X, Y)$ reference frame nondimensionalized by $\rho\pi\Omega^2 r_t^3 l$

$F_x$, $F_y$ = components of the instantaneous lateral force in the $(X, Y)$ reference frame, nondimensionalized by $\rho\pi\Omega^2 r_t^3 l$

$F_n$, $F_t$ = components of the time averaged force on the inducer which are normal and tangential to the whirl orbit respectively and are nondimensionalized by $\rho\pi\Omega^2 r_t^2 l\epsilon$

$l$ = axial blading length of the inducer (hub)

$p_i$ = inlet static pressure

$p_v$ = vapor pressure

$\Delta p_t$ = total pressure rise between inlet and outlet

$Q$ = flow rate

$r_t$ = inducer tip radius

$u_t$ = inducer tip speed, $r_t\Omega$

$x$, $y$ = instantaneous coordinates of the inducer center in the fixed reference frame, nondimensionalized by $r_t$

$\dot{x}$, $\dot{y}$ = time derivatives of $x$ and $y$, nondimensionalized by $r_t\Omega$

$\ddot{x}$, $\ddot{y}$ = acceleration, nondimensionalized by $r_t\Omega^2$

$[K] = \begin{bmatrix} K_{xx} & K_{xy} \\ K_{yx} & K_{yy} \end{bmatrix}$ = generalized stiffness matrix, nondimensionalized by $\rho\pi\Omega^2 r_t^2 l$

$[C] = \begin{bmatrix} C_{xx} & C_{xy} \\ C_{yx} & C_{yy} \end{bmatrix}$ = generalized damping matrix, nondimensionalized by $\rho\pi\Omega r_t^2 l$

$[M] = \begin{bmatrix} M_{xx} & M_{xy} \\ M_{yx} & M_{yy} \end{bmatrix}$ = generalized inertia matrix, nondimensionalized by $\rho\pi r_t^2 l$

### Symbols

$\epsilon$ = radius of the whirl orbit

$\rho$ = density of the working fluid (water)

$\sigma$ = cavitation number, $(p_i - p_v)/(\frac{1}{2}\rho u_t^2)$

$\omega$ = frequency of whirl motion

$\Omega$ = inducer rotational frequency

$\Psi$ = head coefficient, $\Delta p_t/(\rho u_t^2)$

pumps, for example, do indeed show a quadratic variation of the forces with $\omega/\Omega$ (Jery (1986), Franz (1989)). Recent studies of rotordynamic forces due to leakage flows have also shown such a quadratic relation (Guinzburg, 1992). The research presented in this paper investigates whether the rotordynamic forces on an inducer also show a quadratic behavior with $\omega/\Omega$ and the manner in which these forces are affected by cavitation.

It should be noted that the data presented in this paper represent purely fluid induced forces in the sense that the effects of tare forces (the dry weight of the inducer and the centrifugal forces arising by running the inducer in air) and buoyancy have been subtracted from the total force. The steady and unsteady forces presented are mean values obtained by integration over many cycles of rotation and whirl. The normal force ($F_n$) and the tangential force ($F_t$) are normalized by $\rho\pi\Omega^2 r_t^2 l\epsilon$. The steady forces ($F_o$ with components $F_{ox}$ and $F_{oy}$) are normalized by $\rho\pi\Omega^2 r_t^3 l$ where $\rho$ is the density of the fluid, $r_t$ is the inducer tip radius (5.06 cm.) and $l$ is the axial blading length (2.413 cm.). The uncertainties in the data are expressed as the standard deviation of the plotted data. The standard deviations associated with each plot are included in the corresponding plot caption. The variances of the derived quantities were obtained from previous data taken in the facility over 256 cycles of a fundamental reference frequency. The fundamental reference frequency is expressed as $\Omega/J$ (where $\omega/\Omega = I/J$ and $I$, $J$ are integers) at which the orientation of the dynamometer and its location on the whirl orbit geometrically repeat (see also Franz et al., 1990). For the data reported in this paper, the standard deviations were typically less than 0.00091 for the lateral force ($F_o$), and 0.15 and 0.17 for the normal ($F_n$) and tangential ($F_t$) forces respectively.

## Test Matrix

The effects of cavitation were studied at two flow coefficients, $\phi = 0.074$ and $\phi = 0.049$. The flow coefficient ($\phi$) is defined as the ratio of the local axial velocity to tip speed $\phi = Q/(u_t A_i)$ where $Q$ is the flow rate and $A_i$ is the inlet area ($A_i = \pi r_t^2$). These specific flow coefficients were chosen in order to study the effects of flow reversals on the forces ($\phi = 0.049$) and to compare these with the forces at a flow coefficient for which no flow reversals are observed ($\phi = 0.074$). At the flow coefficient of 0.049, upstream tip clearance leakage flow and downstream hub re-entry flows were present. Upstream and downstream flow reversals on this inducer have been studied previously and reported by Bhattacharyya et al. (1993).

For the experiments presented in this paper, the eccentricity was set at $\epsilon = 0.0254$ cm. As a result of this eccentricity the clearance between the inducer blade tip and the housing varied between 0.028 cm. and 0.079 cm. The shaft rotational speed was 3000 rpm and the whirl speed was varied from −0.55 to +0.55 times the shaft speed.

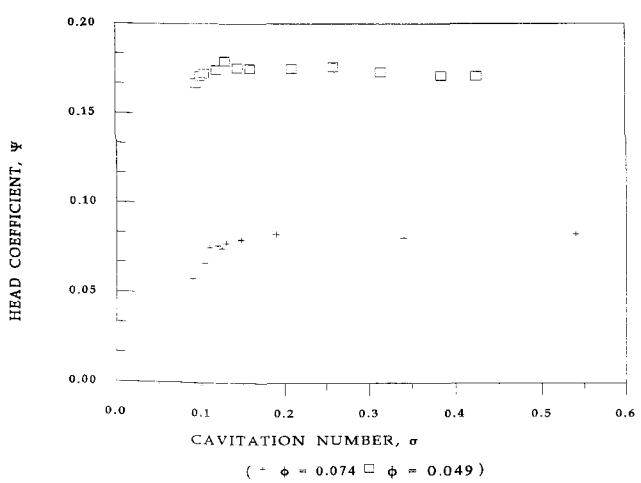


**Fig. 2 Cavitation characteristics of the inducer at 3000 RPM. Uncertainty expressed as a standard deviation: $\psi \pm 0.0056$, $\phi \pm 0.00053$ and $\sigma \pm 0.0039$.**

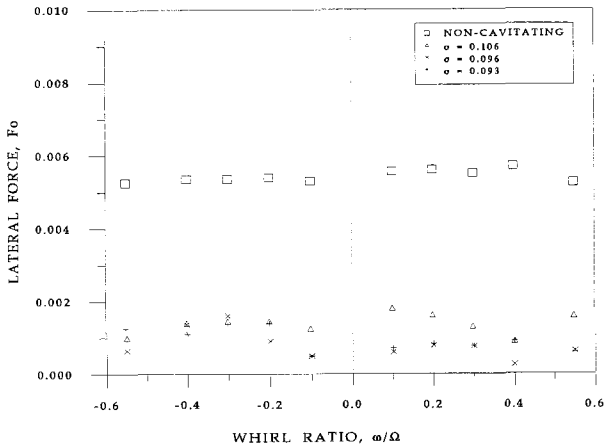


**Fig. 3 Lateral force on the inducer at $\phi = 0.074$ for various cavitation numbers. Uncertainty expressed as a standard deviation: $\|F_o\| \pm 0.00091$, $\omega/\Omega \pm 0.001$, $\phi \pm 0.00053$ and $\sigma \pm 0.0039$.**

The tests on the inducer were conducted in water, deaerated to an air content of less than 3 ppm. The facility includes a pressure regulation system which allows operation at different suction pressures, $p_i$. A conventional cavitation number, $\sigma$, is used to define the non-dimensional suction conditions:

$$\sigma = \frac{(p_i - p_v)}{\frac{1}{2}\rho u_t^2} \tag{9}$$

where $p_v$ is the vapor pressure (at the water temperature) and the tip speed of the inducer is given by $u_t = \Omega r_t$. The results presented are for various cavitation numbers.

## Results

**Cavitation Performance.** The cavitation characteristics of the inducer used for the current experiments are shown in Fig. 2 at $\phi = 0.074$ and $\phi = 0.049$ (3000 rpm). The head coefficient, $\psi$, defined as the ratio $\Delta p_t/(\rho u_t^2)$ where $\Delta p_t$ refers to change in the total pressure, is plotted against various values of the cavitation number. In the case of $\phi = 0.074$, it is seen that as the cavitation number is reduced from noncavitating values, the head coefficient started decreasing at $\sigma = 0.147$. However, there was a slight increase in the head coefficient at $\sigma = 0.113$ followed by a continuous head breakdown below $\sigma = 0.106$. The head coefficient is approximately 0.081 under non-cavitating conditions. At $\sigma = 0.106$ there occurs a 4.9 percent head loss ($\psi = 0.077$). The cavitation characteristics at the lower flow coefficient of $\phi = 0.049$ exhibit a similar behavior.

**Steady Forces Due to Cavitation.** The results of the steady radial force measurements at $\phi = 0.074$ are presented in Fig. 3 for various whirl/shaft speed ratios (−0.55 to +0.55). The steady forces remain constant for a given cavitation number over the range of whirl/shaft speed ratios, but decrease with cavitation number. It is observed that the noncavitating steady forces are much larger than the steady forces with cavitation; reasons for this are discussed later but it should be pointed out that previous research (Bhattacharyya et al., 1992) has shown that the presence of the downstream asymmetry inherent to the test set up causes large lateral forces.

Figure 4 shows the variation of the steady force for various whirl ratios at the flow coefficient of $\phi = 0.049$. The results differ from those obtained for $\phi = 0.074$ in that the cavitating

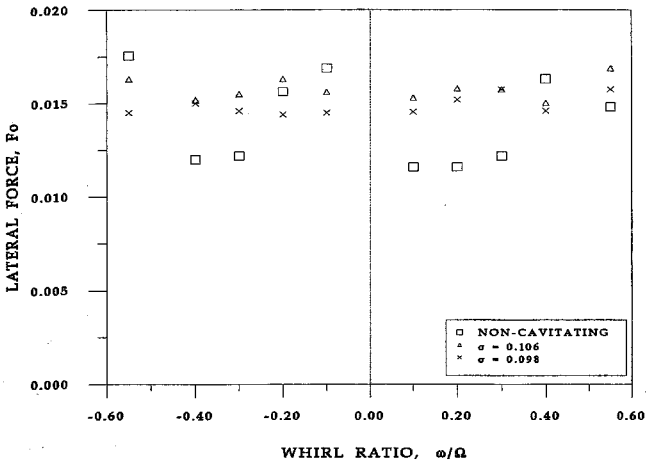


Fig. 4 Lateral force on the inducer at $\phi = 0.049$ for various cavitation numbers. Uncertainty expressed as a standard deviation: $\|F_o\| \pm 0.00091$, $\omega/\Omega \pm 0.001$, $\phi \pm 0.00053$ and $\sigma \pm 0.0039$.

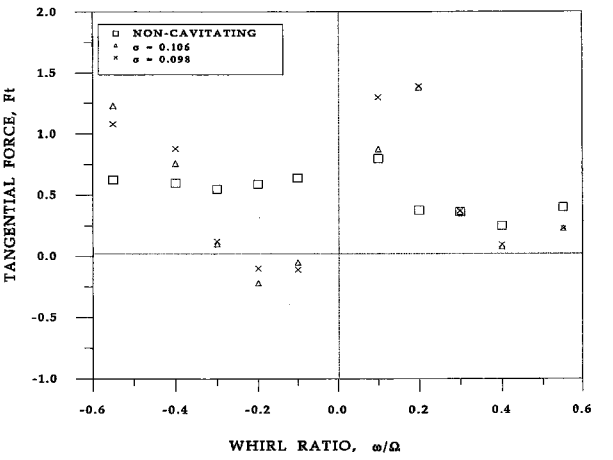


Fig. 6 Tangential force on the inducer at $\phi = 0.049$ for various cavitation numbers. Uncertainty expressed as a standard deviation: $F_t \pm 0.17$, $\omega/\Omega \pm 0.001$, $\phi \pm 0.00053$ and $\sigma \pm 0.0039$.

forces are about the same magnitude as the non-cavitating forces. The large lateral forces at $\phi = 0.049$ are possibly due to the occurrence of reverse flows downstream of the inducer in the presence of a downstream asymmetry inherent to the test set up. Under these conditions, the steady force due to the effect of cavitation cannot be distinguished from the noncavitating steady force.

**Rotordynamic Forces Due to Cavitation.** The rotordynamic forces on the inducer were also obtained at various flow coefficients and cavitation numbers. The tangential force is plotted against whirl frequency ratio, $\omega/\Omega$, for $\phi = 0.074$ in Fig. 5. The significant result obtained is the occurrence of multiple zero crossings. There are some significant differences compared to the non-cavitating force characteristics. One of these is that the tangential force remains negative in a substantial region of negative whirl under cavitating conditions. In fact for $\sigma = 0.106$ and $\phi = 0.074$, the tangential force does not reach a positive value in the negative whirl region (for the range of whirl/shaft speed ratios tested). Another feature of the tangential force is that it exhibits a positive peak in a range of positive whirl frequency ratio around $\omega/\Omega \approx 0.2$. Such a peak is not observed in the noncavitating tangential force at this flow coefficient (with no backflow). In fact, the magnitude of this peak increases as the cavitation number is reduced. The location of the peak also tends to shift to lower whirl/shaft speed ratios. Thus, the extent and manner in which the tangential forces become destabilizing depend on the extent to which the inducer cavitates. At larger positive whirl frequency ratios (especially for $\omega/\Omega > 0.4$), however the tangential force is observed to become increasingly negative (and hence stabilizing) for decreasing cavitation numbers. Thus, for this case, destabilizing tangential forces are generally observed from $\omega/\Omega = 0.0$ to $\omega/\Omega = 0.4$ and in the region $\omega/\Omega < 0.0$.

Figure 6 presents the corresponding results for a flow coefficient $\phi = 0.049$. The variation with whirl frequency ratio are very much similar to those at $\phi = 0.074$, especially in the occurrence of a positive, destabilizing peak around $\omega/\Omega \approx 0.2$. Multiple zero crossings are also evident. However, at this flow coefficient, the tangential force continues to be destabilizing at $\omega/\Omega = 0.55$ for a cavitation number $\sigma = 0.098$ unlike $F_t$ at $\omega/\Omega = 0.55$ for $\phi = 0.074$ (at the same cavitation number).

Figure 7 presents a comparison between the tangential forces at the two flow coefficients for $\sigma = 0.106$. In the region of negative whirl, the forces become more stabilizing for the lower flow coefficient (except for the region between $\omega/\Omega = -0.5$ and $\omega/\Omega \approx -0.3$). The peak force in the region of positive whirl increases in magnitude. The location of this peak also shifts from $\omega/\Omega = 0.3$ at $\phi = 0.074$ to $\omega/\Omega = 0.2$ at $\phi = 0.049$. Another important observation is that for higher positive whirl ratios ($\omega/\Omega > 0.5$), the tangential forces tend to become

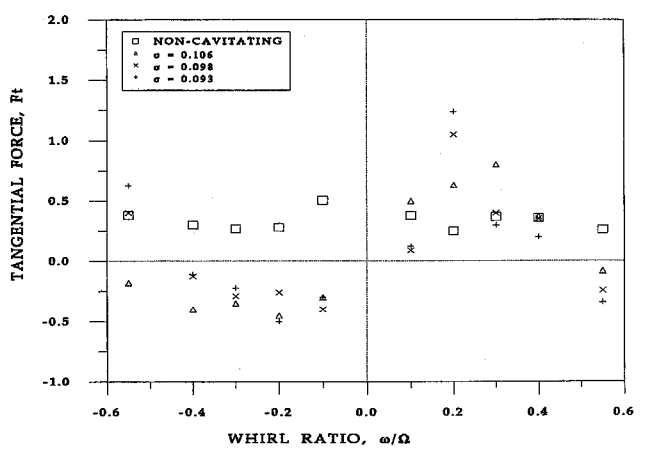


Fig. 5 Tangential force on the inducer at $\phi = 0.074$ for various cavitation numbers. Uncertainty expressed as a standard deviation: $F_t \pm 0.17$, $\omega/\Omega \pm 0.001$, $\phi \pm 0.00053$ and $\sigma \pm 0.0039$.

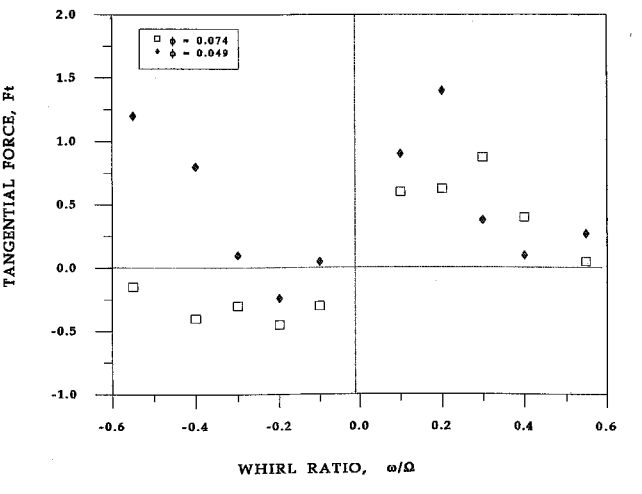


Fig. 7 Comparison of the tangential force on the inducer at a cavitation number $\sigma = 0.106$ for two flow coefficients. Uncertainty expressed as a standard deviation: $F_t \pm 0.17$, $\omega/\Omega \pm 0.001$, $\phi \pm 0.00053$ and $\sigma \pm 0.0039$.

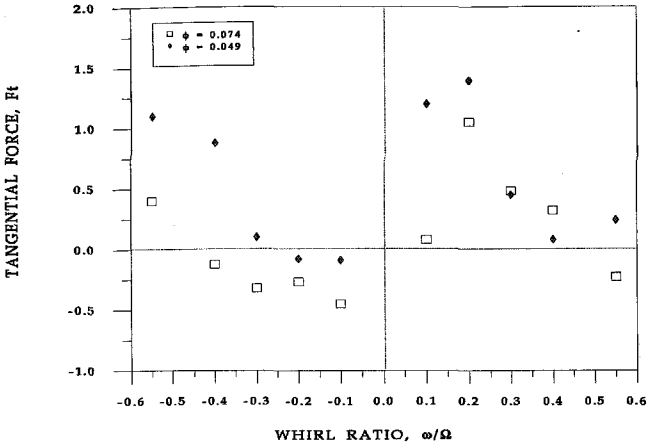


**Fig. 8 Comparison of the tangential force on the inducer at a cavitation number $\sigma = 0.098$ for two flow coefficients. Uncertainty expressed as a standard deviation: $F_t \pm 0.17$, $\omega/\Omega \pm 0.001$, $\phi \pm 0.00053$ and $\sigma \pm 0.0039$.**

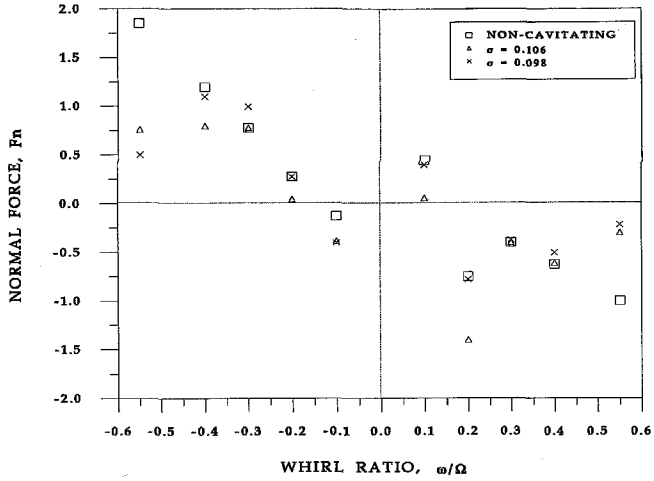


**Fig. 10 Normal forces at flow coefficient $\phi = 0.049$ for various cavitation numbers. Uncertainty expressed as a standard deviation: $F_n \pm 0.15$, $\omega/\Omega \pm 0.001$, $\phi \pm 0.00053$ and $\sigma \pm 0.0039$.**

increasingly destabilizing for the lower flow coefficient (whereas they become stabilizing for the higher flow coefficient).

Similar data for a cavitation number of $\sigma = 0.098$ is shown in Fig. 8. Again a positive peak of the tangential force occurs at $\omega/\Omega \approx 0.2$. For the lower flow coefficient, the range of destabilizing tangential force decreases for negative whirl (approximately $-0.3 < \omega/\Omega < -0.1$ at $\phi = 0.049$ compared to approximately $-0.4 < \omega/\Omega < 0.1$ at $\phi = 0.074$ for $\sigma = 0.098$).

The forces normal to the whirl orbit on the inducer at the flow coefficient of 0.074 have been plotted for different cavitation numbers in Fig. 9. It is observed that the normal forces do not vary significantly with cavitation number once cavitation has been established. However, compared to the non-cavitating data, we observe large and increasingly positive (destabilizing) normal forces with increasing positive whirl frequency ratios. Furthermore, the normal force in the presence of cavitation tends to be of a larger (negative) magnitude than the non-cavitating normal force for the range of whirl frequency ratios between $-0.1$ and $+0.1$. The characteristics of the normal force (with cavitation) in the region of negative whirl ($\omega/\Omega < -0.1$) tends to be similar to the noncavitating normal force behavior.

Figure 10 presents similar data for the lower flow coefficient of 0.049. In this case the normal force behavior displays multiple zero crossings. A significant feature is the occurrence of negative peaks at all the cavitation numbers (including the non-cavitating case). It is also noted that the normal force decreases for $\omega/\Omega < -0.4$ and increases for $\omega/\Omega > +0.4$ with decreasing cavitation numbers.

The normal forces at a given cavitation number, $\sigma = 0.106$, and two flow coefficients are compared in Fig. 11. As in the case of the tangential forces, a decrease in the flow coefficient clearly causes changes in the normal force. The number of zero crossings increase with a decrease in the flow coefficient and an additional region of positive (destabilizing) force occurs around $\omega/\Omega = 0.1$. Another significant effect caused by decreasing the flow coefficient is the appearance of a negative peak in the normal force in a region of positive whirl; at $\phi = 0.049$, $\sigma = 0.106$ this peak occurs around $\omega/\Omega \approx 0.2$. It is also observed at lower flow coefficients that the normal force tends to remain negative over a longer range of positive whirl frequencies. A comparison similar to that of Fig. 11 is shown in Fig. 12, but at the lower cavitation number $\sigma = 0.098$. An increase in the number of zero crossings of the force is observed at the lower flow coefficient. A positive (destabilizing) peak appears at $\omega/\Omega \approx 0.1$ for the lower flow coefficient at this cavitation number and along with a negative peak at $\omega/\Omega \approx 0.2$.

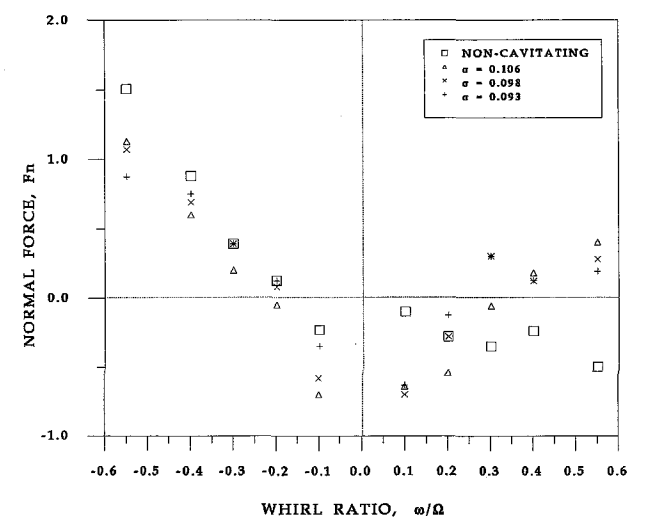


**Fig. 9 Normal forces at flow coefficient $\phi = 0.074$ for various cavitation numbers. Uncertainty expressed as a standard deviation: $F_n \pm 0.15$, $\omega/\Omega \pm 0.001$, $\phi \pm 0.00053$ and $\sigma \pm 0.0039$.**

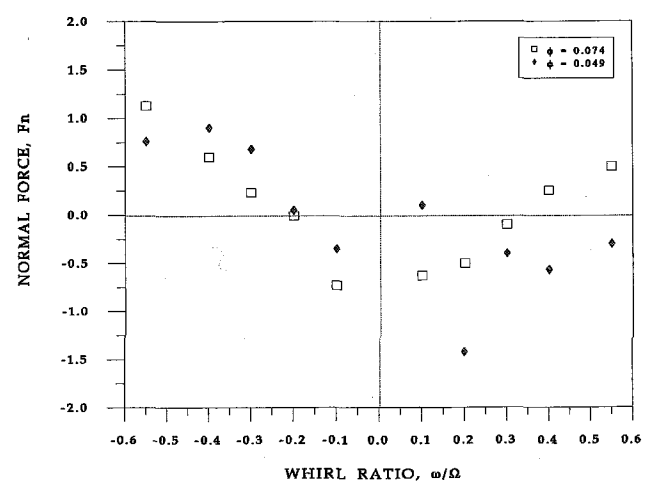


**Fig. 11 Comparison of the normal force on the inducer at a cavitation number $\sigma = 0.106$ for two flow coefficients. Uncertainty expressed as a standard deviation: $F_n \pm 0.15$, $\omega/\Omega \pm 0.001$, $\phi \pm 0.00053$ and $\sigma \pm 0.0039$.**

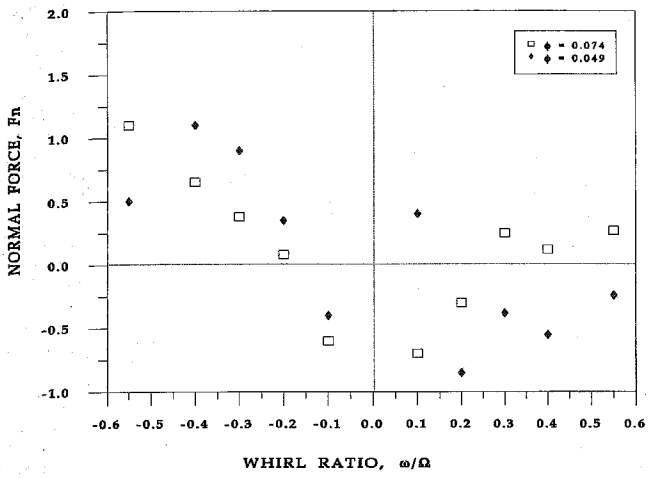


**Fig. 12 Comparison of the normal force on the inducer at a cavitation number $\sigma = 0.098$ for two flow coefficients. Uncertainty expressed as a standard deviation: $F_n \pm 0.15$, $\omega/\Omega \pm 0.001$, $\phi \pm 0.00053$ and $\sigma \pm 0.0039$.**

## Discussion

The results presented in this paper show that cavitation has a significant effect on inducer rotordynamic forces. The destabilizing rotordynamic forces could lead to failure of the device in which the inducer is being used. It is therefore important to gain a fundamental understanding of the nature of these forces, in order to facilitate changes in the design and/or operating conditions of the machine.

A simple helical inducer was chosen for these preliminary tests. The effect of the geometry of inducers of this type on the cavitation performance have been reported previously (Acosta, 1958). The mechanism of head breakdown has also been studied by researchers such as Jakobsen (1964).

The influence of the flow coefficient on non-cavitating steady forces has been reported earlier (Bhattacharyya et al., 1992). It was shown that the presence of a downstream asymmetry causes significantly large steady forces due to the occurrence of a downstream flow reversal. The current experiments with cavitation were conducted with the same downstream asymmetry which is inherent to the system. This is the cause of the large non-cavitating steady force seen in Figs. 3 and 4. However, it may be noted that the downstream flow reversal for $\phi = 0.074$ is probably only incipient since previous flow visualization on the hub did not reveal re-entry flows on the hub (there was no observable upstream swirling backflow either). Furthermore, the occurrence of cavitation at this higher flow rate actually results in a lower net steady force. It may be speculated that this occurs because of the lower pumping work being done on the fluid because of cavitation. In the case of the lower flow coefficient, the steady force always remains high regardless of the extent of cavitation.

The unsteady force data suggest that flow reversals can also have significant consequences for rotordynamic forces. For non-cavitating flow the tangential forces are destabilizing for positive whirl at both flow coefficients. The noncavitating tangential force shows a destabilizing peak for positive whirl at $\omega/\Omega = +0.1$ for the lower flow coefficient. A similar observation was made on noncavitating inducers by Arndt and Franz (1986). A more dramatic effect of the flow coefficient is observed in cavitating flow. In the case of the inducer tested, the effect of lowering the flow coefficient increased the region of destabilization (positive $F_t$) for positive whirl. Furthermore, the effect of a decreased flow did not change the location of the peak, but rather led to an increase in its magnitude. For negative whirl, the higher flow coefficient was more destabilizing. This is an interesting observation especially when the current results are compared to the data obtained previously by Karyeaclis et al. (1989) on a four bladed inducer (called the SEP inducer) with a hub which increases substantially between inlet and discharge. The inducer installation of the SEP inducer was similar to the current configuration. In the case of the SEP inducer, the tangential forces were less destabilizing for the lower flow coefficient for positive whirl frequencies, unlike the current results. Karyeaclis et al. (1989) argued that for a given cavitation number, larger forces could be expected at the higher flow coefficient because it is closer to the performance breakdown point. The current results do not show the same trend; thus it appears that the *geometry* of the inducer has a significant effect on the rotordynamic forces. Further, the current results show a tangential force peak at $\omega/\Omega = +0.2$ rather than at $\omega/\Omega = +0.5$ observed for the SEP tests. In Karyeaclis et al. (1989) it was argued that the peak at $\omega/\Omega = +0.5$ was a sympathetic resonance with the fluid behind the inducer which rotates at half the shaft speed. In the current tests, however, the peak occurs at much less than half the shaft speed. In the case of the normal forces, the effect of a reduction in the flow coefficient was an increase in the number of positive and negative peaks. These differences in the characteristics of rotordynamic forces with whirl frequencies under cavitating conditions probably stem from the differences in internal flows and reverse flow patterns caused by the geometry differences in inducers.

The effect of cavitation on the tangential forces at a given flow coefficient is significant. It is observed that for decreasing cavitation numbers, the magnitude of the peak in the force at $\omega/\Omega = +0.2$ increases and becomes narrower. Thus the range of destabilizing forces decreases. This is the reverse of the trend to that observed by Karyeaclis et al. (1989) for the SEP inducer where larger forces were accompanied by larger instability regions. Also, in the case of the current inducer the tangential forces with increasing cavitation become increasingly stabilizing for negative whirl.

Another important observation is that the data for $F_t$ and $F_n$ as a function of $\omega/\Omega$ do not exhibit the kind of quadratic functional behavior which is normally assumed in many rotordynamic models. Rather, as has been reported previously (Karyeaclis et al., 1989) much higher order polynomials would be required to approximate the forces. Thus the representation of the components of the rotordynamic matrix $[A]$ (as given in Eq. (4)) does not hold for the cavitating inducer. Consequently, the generalized stiffness, damping and inertia matrices for the inducer cannot be determined. Instead, rotordynamic analysis of the inducer must include fluid-induced forces which are more general functions of the whirl frequency ratio.

## Conclusions

(1) This paper reports an experimental investigation of rotordynamic forces on a simple three bladed, helical, axial flow inducer with a constant hub ratio. The influence of cavitation and off-design flow rates on these forces are presented. Rotordynamic forces are destabilizing at various whirl ratios, when the inducer is whirled in a circular orbit at a fraction of its rotational speed. An understanding of these forces is important to determine dynamic stability of high speed pumping systems such as the high pressure turbopumps used in the space shuttle main engine.

(2) Cavitation has important consequences for fluid-induced rotordynamic forces generated by inducers. These forces can become destabilizing at both positive and negative whirl frequencies. Increasing levels of cavitation could cause an increase in destabilizing forces.

(3) The rotordynamic forces do not exhibit a quadratic functional behavior (typical of centrifugal impellers) and hence the conventional generalized stiffness, damping and inertia matrices cannot be determined.

(4) The internal flow patterns and flow reversals associated with reduced flow coefficients appear to have a significant bear-

ing on these forces. Lower flow coefficients, characterized by upstream backflows and downstream re-entry flows, are also associated with increases in destabilizing peaks of rotordynamic forces. The flow patterns are, in turn, dependent on the inducer geometry and the dependence of the forces on the extent of cavitation must be included in design considerations.

Given that analytical techniques are, as yet, unable to predict unsteady cavitating forces in turbomachinery, the experimental data obtained in the current research provides an appropriate starting point for the understanding of these complex forces in axial flow inducers.

## Acknowledgment

The authors would like to thank the NASA George C. Marshall Space Flight Center for sponsoring this project under contract no. NAG8-118, Henry L. Stinson, contract monitor.

## References

Acosta A. J., 1958, "An Experimental Study of Cavitating Inducers," *Proceedings 2nd Symposium on Naval Hydrodynamics,* Washington, D.C., pp. 533–557.

Acosta A. J., 1993, "Flow in Inducer Pumps, An Aperçu," *Proceedings 4th International Symposium on Transport Phenomena and Dynamics Of Rotating Machinery,* Honolulu, Vol. A., pp. 1–13.

Arndt N., and Franz R., 1986, "Observations of Hydrodynamic forces on Several Inducers including the SSME LPTOP," Report No. E249.3, Division of Engineering and Applied Sciences, California Institute of Technology, Pasadena, CA.

Bhattacharyya A., Acosta A. J., Brennen C. E., and Caughey T. K., 1992, "The Formation of Backflow and its Consequences on the Lateral Forces in Axial Flow Impellers," *Abstracts of the ASME Fluids Engineering Conference,* Los Angeles, FED-Vol. 133, pp. 237–239.

Bhattacharyya A., Acosta A. J., Brennen C. E., and Caughey T. K., 1993, "Observations on Off-Design Flows in Axial Flow Inducers," *Proceedings Pumping Machinery Symposium,* ASME Fluids Engineering Conference, Washington D.C., FED-Vol. 154, pp. 135–141.

Franz R., 1989, "Experimental Investigation of the Effect of Cavitation on the Rotordynamic Forces on a Whirling Centrifugal Pump Impeller," Ph.D. thesis, Division of Engineering and Applied Sciences, California Institute of Technology, Pasadena, California.

Franz R., Acosta A. J., Brennen C. E., and Caughey T. K., 1990, "The Rotordynamic Forces on a Centrifugal Pump Impeller in the Presence of Cavitation," ASME JOURNAL OF FLUIDS ENGINEERING, Vol. 112, No. 3, pp. 264–271.

Guinzburg A., 1992, "Rotordynamic Forces Generated by Discharge-to-Suction Leakage Flows in Centrifugal Pumps," Ph.D. thesis, Division of Engineering and Applied Sciences, California Institute of Technology, Pasadena, CA.

Jakobsen J. K., 1964, "On the Mechanism of Head Breakdown in Cavitating Inducers," ASME *Journal of Basic Engineering,* pp. 291–305.

Jery B., 1986, "Experimental Study of Unsteady Hydrodynamic Force Matrices on Whirling Centrifugal Pump Impellers," Ph.D. thesis, Division of Engineering and Applied Sciences, California Institute of Technology, Pasadena, California.

Kamijo K., Shimura T., and Watanabe M., 1977, "An Experimental Investigation of Cavitating Inducer Instability," *Proceedings ASME Winter Annual Meeting,* Atlanta.

Karyeaclis M. P., Miskovish R. S., and Brennen C. E., 1989, "Rotordynamic Tests in Cavitation of the SEP Inducer," Report No. E200.27, Division of Engineering and Applied Sciences, California Institute of Technology, Pasadena, CA.

Lakshminarayana B., 1972, "Visualization Study of Flow in an Axial Flow Inducer," ASME *Journal of Basic Engineering,* pp. 777–787.

Lakshminarayana B., 1982, "Fluid Dynamics of Inducers—A Review," ASME JOURNAL OF FLUIDS ENGINEERING, Vol. 104, pp. 777–787.

Rosenmann W., 1965, "Experimental Investigations of Hydrodynamically Induced Shaft Forces with a Three Bladed Helical Inducer," *Proceedings ASME Symposium on Cavitation in Turbomachinery,* pp. 172–195.